Cell Stem Cell

Short article

8C-like cells capture the human zygotic genome activation program *in vitro*

Graphical abstract

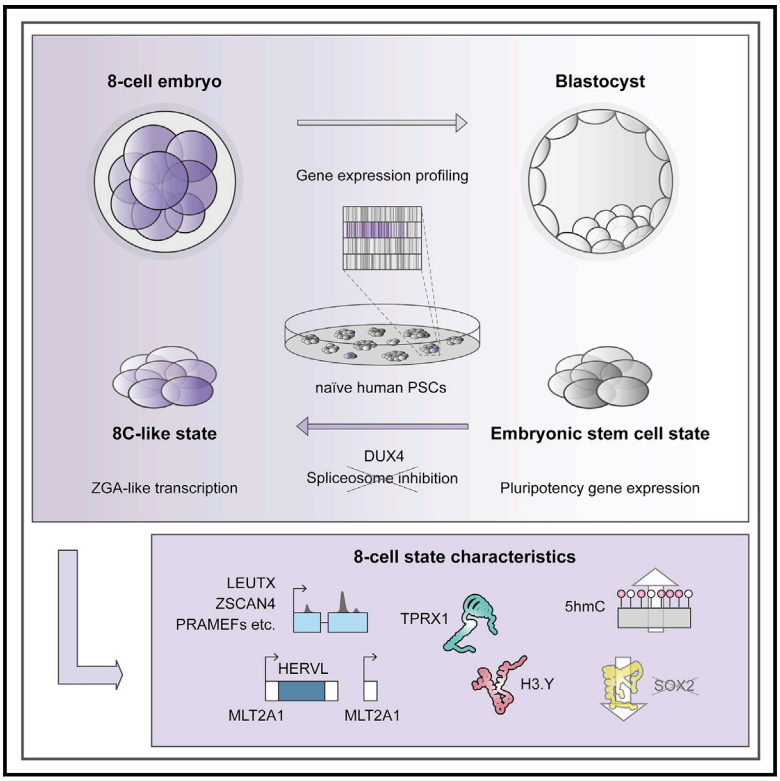

Highlights

- ZGA genes and transposable elements are expressed in 8CLCs but not in naive stem cells
- DUX4 overexpression and spliceosome inhibition induce ZGA-like transcription
- 8CLC marker proteins TPRX1 and H3.Y are expressed in 8-cell human embryos
- 8CLCs can be used to study human ZGA-like programs *in vitro*

Authors

Jasmin Taubenschmid-Stowers, Maria Rostovskaya, Fátima Santos, ..., Felix Krueger, Jennifer Nichols, Wolf Reik

Correspondence

jasmin.stowers@babraham.ac.uk (J.T.-S.), wolf.reik@babraham.ac.uk (W.R.)

In brief

Taubenschmid-Stowers et al. discover human 8-cell-like cells that express transcription programs resembling zygotic genome activation *in vitro*. As these 8CLCs express genes, endogenous retroviruses, and proteins similar to 8-cell embryos, they can be used to study the molecular principles of human embryonic genome activation in stem cells *in vitro*.

Taubenschmid-Stowers et al., 2022, Cell Stem Cell *29*, 449–459
March 3, 2022
https://doi.org/10.1016/j.stem.2022.01.014

CellPress

Cell Stem Cell

CellPress
OPEN ACCESS

Short article

8C-like cells capture the human zygotic genome activation program *in vitro*

Jasmin Taubenschmid-Stowers,[1,*] Maria Rostovskaya,[1] Fátima Santos,[1,2] Sebastian Ljung,[1] Ricard Argelaguet,[1] Felix Krueger,[1] Jennifer Nichols,[2,3,4] and Wolf Reik[1,2,5,6,*]

[1]Epigenetics Programme, Babraham Institute, Cambridge CB22 3AT, UK
[2]Centre for Trophoblast Research, University of Cambridge, Cambridge CB2 3EG, UK
[3]Wellcome-MRC Cambridge Stem Cell Institute, University of Cambridge, Cambridge CB2 0AW, UK
[4]Department of Physiology, Development and Neuroscience, University of Cambridge, Cambridge CB2 3EL, UK
[5]Wellcome Trust Sanger Institute, Hinxton, Cambridge CB10 1SA, UK
[6]Lead contact
*Correspondence: jasmin.stowers@babraham.ac.uk (J.T.-S.), wolf.reik@babraham.ac.uk (W.R.)
https://doi.org/10.1016/j.stem.2022.01.014

SUMMARY

The activation of the embryonic genome marks the first major wave of transcription in the developing organism. Zygotic genome activation (ZGA) in mouse 2-cell embryos and 8-cell embryos in humans is crucial for development. Here, we report the discovery of human 8-cell-like cells (8CLCs) among naive embryonic stem cells, which transcriptionally resemble the 8-cell human embryo. They express ZGA markers, including *ZSCAN4* and *LEUTX*, and transposable elements, such as *HERVL* and *MLT2A1*. 8CLCs show reduced SOX2 levels and can be identified using TPRX1 and H3.Y marker proteins *in vitro*. Overexpression of the transcription factor DUX4 and spliceosome inhibition increase human ZGA-like transcription. Excitingly, the 8CLC markers TPRX1 and H3.Y are also expressed in ZGA-stage 8-cell human embryos and may thus be relevant *in vivo*. 8CLCs provide a unique opportunity to characterize human ZGA-like transcription and might provide critical insights into early events in embryogenesis in humans.

INTRODUCTION

Mammalian embryogenesis begins shortly after fertilization with the formation of the totipotent zygote. Totipotency is established through epigenetic and transcriptional remodeling and licenses the formation of all cell types of the developing organism (Tarkowski, 1959). Zygotic or embryonic genome activation (ZGA, EGA), after a smaller minor wave, marks the first major wave of transcription in the totipotent mouse 2-cell and human 8-cell embryo, and is essential for the ensuing first lineage decisions (Aoki et al., 1997; Asami et al., 2021; Braude et al., 1988; Kigami et al., 2003; Latham and Schultz, 2001; Lee et al., 2014; Vassena et al., 2011). Failure to accurately remodel the epigenome or activate embryonic transcription contributes to substantial lethality of human pre-implantation embryos, but it may also have longer term consequences later in development (Niakan et al., 2012). Understanding the molecular events regulating genome activation is therefore important for human reproduction and health. The direct study of human embryos, however, is practically and ethically limited.

To study mammalian early development *in vitro*, mouse and human pluripotent or embryonic stem cells (PSCs, ESCs) have been used as model systems (Evans and Kaufman, 1981; Thomson et al., 1998). Naive human PSCs correspond to cells of the pre-implantation epiblast, whereas primed ones represent post-implantation-stage cells (Huang et al., 2014; Nakamura et al., 2016; Theunissen et al., 2016). Moreover, among naive mouse ESCs, a small subpopulation of so-called 2C-like cells (2CLCs) has been described, which closely resembles the totipotent 2-cell embryo *in vivo* (Macfarlan et al., 2012). Although these cells have already undergone ZGA in an embryo context before their derivation from mouse blastocyst, they re-activate a 2-cell or ZGA-like transcriptional and epigenetic program in culture and have been shown to cycle in and out of this state from mouse ESCs (Macfarlan et al., 2012; Rodriguez-Terrones et al., 2018). 2CLCs can be identified based on the upregulation of the endogenous retrovirus MERVL and can be used to study ZGA-like transcription *in vitro* (Alda-Catalinas et al., 2020; Eckersley-Maslin et al., 2016; Ishiuchi et al., 2015; Macfarlan et al., 2012). Moreover, 2CLCs have been reported to possess greater developmental potential than conventional ESCs and are able to contribute to extra-embryonic lineages during mouse development (Macfarlan et al., 2012; Shen et al., 2021). To date, no equivalent *in vitro* human 2-cell- or 8-cell-like cell type has been described.

Here, we report the discovery of human 8-cell-like cells, 8CLCs, specifically among human naive ESCs. 8CLCs express ZGA marker genes such as *ZSCAN4, LEUTX, TPRX1*, and *PRAMEFs*. Their transcriptome, including transposon expression profile, closely resembles that of human 8-cell embryos. 8CLCs are characterized by upregulation of the DNA methylation

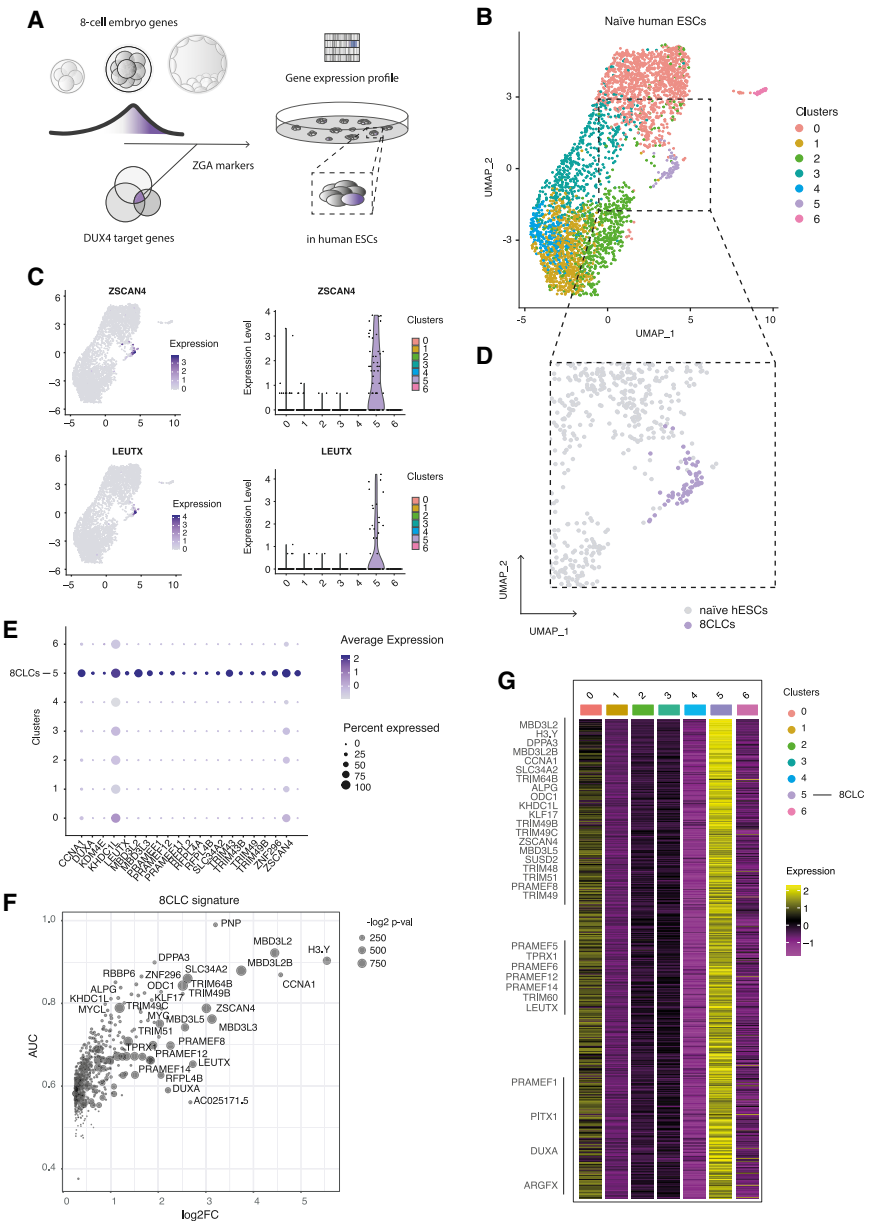

Figure 1. ZGA marker expression in 8CLCs and naive hESCs

(A) Schematic of identifying a system to study human ZGA-like programs *in vitro*.

(B) UMAP of naive HNES1 hESCs cultured in PXGL. Cell clustering is based on normalized, scaled single-cell RNA expression data.

(C) Normalized, scaled gene expression of *ZSCAN4* and *LEUTX* in naive human ESCs, visualized using UMAPs (left) or Violin plots of clustered cells (right) (clusters 0, 1, 2, 3, 4, 5, and 6 contain n = 1,237, 709, 611, 517, 251, 55, and 30 cells, respectively).

(D) UMAP of cluster 5 cells, highlighted as "8C-cell-like cells," "8CLCs," comprising ~1.6% (55 of 3,410) of total naive cells.

(E) Dotplots of ZGA marker frequency and average expression level of clustered naive hESCs.

(F) Gene expression signature of cluster 5 cells, or 8CLCs, as determined by the "findmarkers" function in Seurat. AUC, area under curve; LOG2FC, $\log_2$ fold-change; $-\log_2$ p val, negative $\log_2$ p value.

(G) Heatmap of normalized, scaled average expression of 8CLC (cluster 5) markers (rows) in naive hESC clusters (columns, cluster 0–6).

regulator *DPPA3* and lower SOX2 protein levels. 8CLCs can be identified *in vitro* by the expression of the protein marker TPRX1. Overexpression of the transcription factor DUX4 not only increases ZGA-like gene expression but also enhances TPRX1-positive 8CLC formation. We have thus uncovered a unique *in vitro* cell state, 8CLCs, which allows us to study human ZGA-like transcriptional programs *in vitro*.

RESULTS

ZGA markers are expressed in 8CLCs among naive human PSCs

To study functionally the molecular events of human ZGA regulation, we sought to discover an *in vitro* model system. We defined ZGA markers from human embryo RNA sequencing (RNA-seq) data and overexpression studies of the ZGA-associated transcription factor (TF) DUX4 in different cell lines (De Iaco et al., 2017; Hendrickson et al., 2017; Petropoulos et al., 2016) (Figure 1A). From human embryo transcriptomes, we chose features that were overrepresented at the 8-cell stage during genome activation (embryonic day 3, E3) (Petropoulos et al., 2016) (Figure S1A). These features include known ZGA markers, such as the TF *ZSCAN4* (Falco et al., 2007; Zalzman et al., 2010), the eutherian-specific paired-like homeodomain protein *LEUTX* (Jouhilahti et al., 2016), as well as the *TRIM* and *PRAMEF* superfamily of genes, all of which are specifically expressed in 8-cell-stage embryos (Figures S1A–S1D). To refine this gene set, we integrated overexpression data of *DUX4*, one of the few transcription factors that have been implicated in mouse and human ZGA (De Iaco et al., 2017; Hendrickson et al., 2017; Yoshihara et al., 2021). It is specifically expressed in the 4-cell human embryo just prior to ZGA initiation and has been suggested to act as an activator of ZGA-like transcription. Endogenous upregulation, as well as overexpression of exogenous *DUX4* in human primary cells and different cell lines, leads to the upregulation of a common set of genes, almost all of which are expressed specifically at the time of human ZGA (Figures S1E and 1F) (Hendrickson et al., 2017; Jiang et al., 2020; Yao et al., 2014). We combined the human embryo *in vivo* data with the *DUX4* overexpression studies to define a common set of human ZGA markers (Table S1) that can be studied *in vitro*.

We next assessed the presence of these markers in single-cell transcriptome data of cultured human embryonic stem cells. We first assessed ZGA-like transcription in human embryo-derived naive HNES1 cells cultured under PXGL conditions (Guo et al., 2017; Guo et al., 2016; Rostovskaya et al., 2019). Single-cell expression data revealed several distinct populations of cells as judged by dimensionality reduction and clustering (Figure 1B). Notably, a distinct subset of 55 cells out of 3,410 (cluster 5 in our dataset) showed clear upregulation of several ZGA-like transcripts simultaneously (Figures 1C and 1D). These transcripts did not only include ZGA genes, such as *LEUTX* and *ZSCAN4*, but also extended to most previously identified ZGA markers, including *DUXA*, *MBD3L3*, and *TRIM49* (Figure S1G). The level of ZGA gene expression and percentage of cells expressing those markers varied within the cluster (Figures 1D and 1E) but was in general consistently high in cells belonging to cluster 5 (Figures S1H–S1K). We termed cluster 5 cells "8-cell-like cells," or "8CLCs."

8CLCs can be discriminated from the remaining naive ESCs based on the expression of more than 700 markers that are specifically upregulated in cluster 5 (Figures 1F and 1G). This 8CLC signature includes all previously selected ZGA markers (*ZSCAN4*, *LEUTX*, *PRAMEF1*, *MBD3L3,* etc.) but notably also additional factors, such as the maternal and zygotic DNA demethylation regulator *DPPA3* (Huang et al., 2017), the naive pluripotency marker *KLF17* (Blakeley et al., 2015; Guo et al., 2016), the histone variant *H3.Y* (a recently described *DUX4* target) (Resnick et al., 2019), and the eutherian-specific genome activation associated factor *TPRX1* (Madissoon et al., 2016; Maeso et al., 2016) (Figure 1F; Table S2). 8CLC signature genes are not detected or expressed at low levels in the other subpopulations of clustered naive ESCs (Figure 1G). These analyses show that 8CLCs are characterized by a distinct and unique gene expression signature within a subpopulation of naive human pluripotent stem cells.

We next asked if the presence of 8CLCs was specific to the embryo-derived HNES1 cell line or if they could be found in other naive hPSCs as well. We analyzed single-cell expression data of human H9-derived NK2 PSCs that were genetically reprogrammed from primed cells via overexpression of *NANOG* and *KLF2* and cultured in t2iLGö (Messmer et al., 2019). Indeed, naive NK2 cells also contained a distinct subpopulation of 8CLCs that upregulate ZGA markers (*TRIM49*, *MBD3L3*, and *LEUTX*) and 8CLCs signature genes (*DPPA3* and *SUSD2*) as compared with the remaining naive hPSCs (Figures S1L and S1M). In both single-cell RNA-seq datasets, ZGA-like transcriptome-expressing cells comprise around 1.5% of the population of total naive cells, a similar proportion to mouse 2C-like cells (Macfarlan et al., 2012).

We further compared ZGA-like transcription under different naive and primed culture conditions (Theunissen et al., 2016). In addition to PXGL cultured cells, 5iLA, 4iLA, and t2iLGö cells are considered truly naive as they resemble cells of the human pre-implantation epiblast *in vivo*. NHSM media, primed culture conditions (WIBR cells), and differentiated neuronal precursor cells (NPCs) represent later stages in development (Theunissen et al., 2016; Nakamura et al., 2016). ZGA markers and most 8CLC signature genes are found highly expressed in naive 5iLA, 4iLA, and t2iLGö cells but are lower in pseudo-naive (NHSM), primed (WIBR), and differentiated cells (NPCs) (Figure S2A). Similarly, ZGA markers and 8CLCs signature are downregulated from naive (PXGL) to primed (E8 or XAF—containing XAV939, Activin A, and FGF2, similar to mouse EpiSC medium) transition of HNES1 cells, as well as chemically reset cR-H9-EOS cells (Figure S2B) (Rostovskaya et al., 2019; Sumi et al., 2013). These data suggest that 8CLCs and ZGA-like transcription can be found in naive-state PSCs but not in primed or differentiated cells.

8CLC transcription resembles that of human 8-cell embryos

We next compared the 8CLC transcriptome *in vitro* with human 8-cell embryos *in vivo*. We analyzed gene expression profiles at different stages and from different studies of human pre-implantation development (Petropoulos et al., 2016; Stirparo et al., 2018; Xue et al., 2013; Yan et al., 2013). These analyses showed that both ZGA markers and 8CLC signature genes peak in 8-cell human embryos during ZGA (E3 embryos) and are downregulated thereafter in morulae (E4 embryos) (Figures 2A, 2B, S2C, and S2D). By contrast, whereas the top 8CLC signature genes are upregulated during ZGA (Figure S2E), naive marker genes that are lowly expressed in 8CLCs are downregulated during ZGA and are only expressed at later stages in blastocysts (E5–E7) (Figure S2F). Moreover, comparison of ZGA markers in single-cell expression data of conventional, naive, 8CLCs and the human embryo (Petropoulos et al., 2016) shows strong similarity between 8CLCs and the 8-cell-stage embryo (E3) (Figure 2C), with almost half of the 8CLC signature genes overlapping with 8-cell human embryo markers (Figure 2D). Notably, markers that differ between the latter include naive stem cell markers, such as *SUSD2* and alkaline phosphatase *ALPG* and *ALPP*, whereas 8-cell embryo genes include maternal factors, such as the growth differentiation factor *GDF9*, Zona pellucida proteins *ZP1 –ZP4* and the human pre-implantation development associated *NLRP* family of proteins (*NLRP4, NLRP9, NLRP11*, and *NLRP13*) (Table S3). Finally, when we combined single-cell sequencing data of naive ESCs and human embryos, most 8CLCs clustered together with 8-cell-stage embryos (E3) and morula cells (E4), whereas naive hESCs clustered together with blastocyst-stage cells (E5–E7) (Figures 2E and 2F). These analyses confirm a remarkable similarity in gene expression patterns of 8CLCs *in vitro* and human 8-cell embryos *in vivo*.

ZGA-specific TF motifs and transposable elements are enriched in 8CLCs

We next wanted to identify candidate TF signatures that might regulate ZGA-like transcription. We analyzed potential binding sites in the genome surrounding (±10 kb) 8CLC signature genes and identified several enriched motifs, such as *DUX4*, *DUXA*, and *KLF17* (Figures 3A and 3B). Notably, *KLF17* is upregulated in 8CLCs (Figure 3C) and 8-cell human embryos (Figure 2B) (Blakeley et al., 2015). *DUX4-, DUXA-,* and *KLF17*-binding motifs have also been reported to be highly accessible during human ZGA (Bentsen et al., 2020; Liu et al., 2019). Thus, transcriptional regulation of ZGA signature genes *in vivo* could potentially also regulate 8CLC-formation *in vitro*.

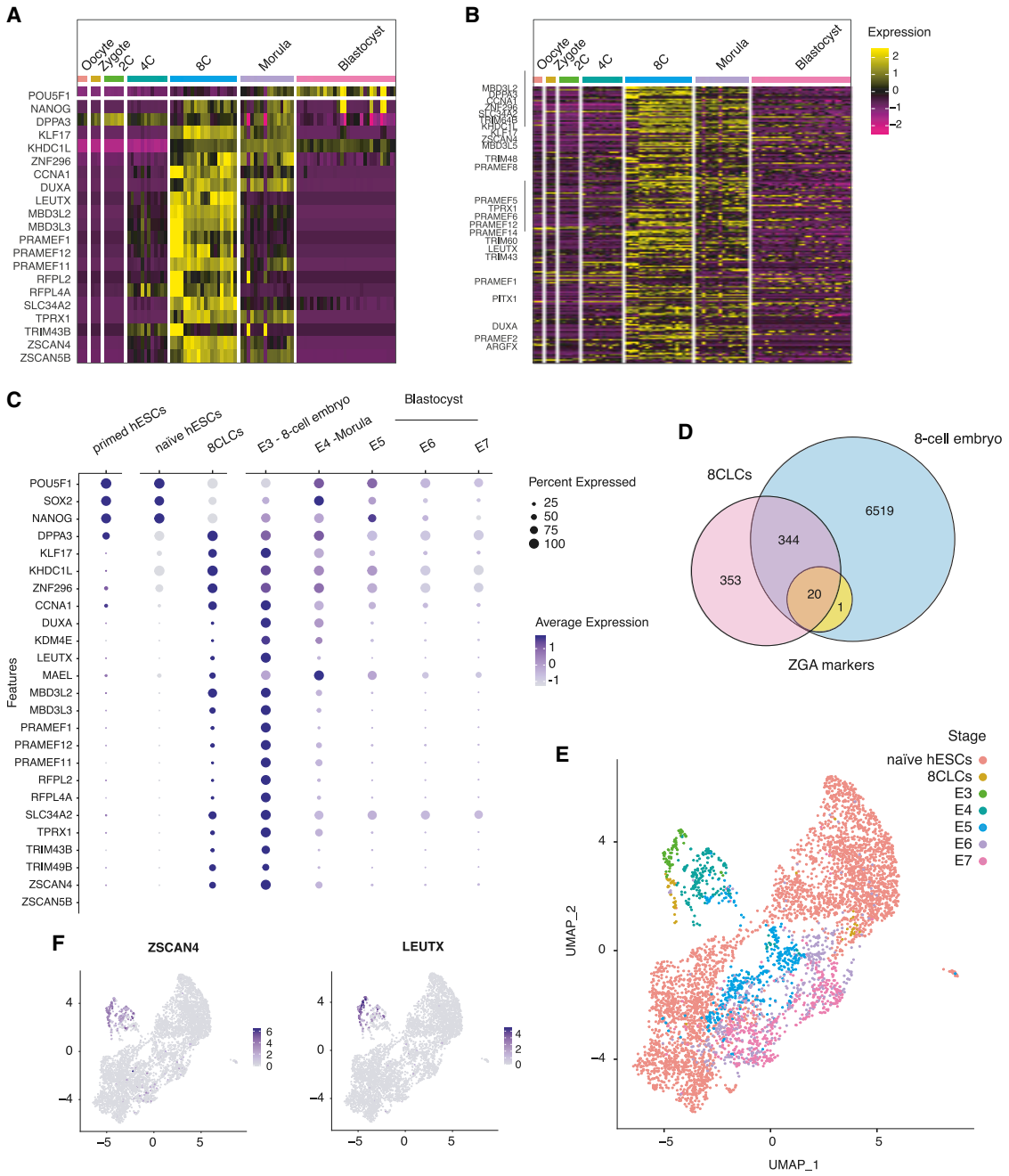

Figure 2. 8CLCs transcriptome signature in human embryos

(A and B) (A) Heatmap of normalized, scaled expression of ZGA markers and pluripotency genes, as well as (B) 8CLCs signature genes (rows) in human pre-implantation embryo cells (columns) (Yan et al., 2013).

(C) Dotplots of frequency and average expression of ZGA markers and pluripotency genes in 8CLCs, naive hPSCs, primed hPSCs (Rostovskaya et al., 2019), and human 8-cell (E3) to blastocyst (E7) stage embryos (Petropoulos et al., 2016).

(D) Overview of shared ZGA markers (n = 21), 8CLCs genes (n = 717), and 8-cell embryo markers (n = 6,894) (Petropoulos et al., 2016).

(E) Clustering of individual 8CLCs, naive hPSCs, and 8-cell to blastocyst-stage embryo cells (E3–E7) (Petropoulos et al., 2016) depicted on a UMAP. Datasets have been combined and merged in Seurat.

(F) *ZSCAN4* and *LEUTX* expression levels in clustered 8CLCs, naive hESCs, and human embryos (E3–E7) (Petropoulos et al., 2016).

We also assessed the transposon expression landscape in 8CLCs. Endogenous retroviral or transposable elements, such as MERVL, have been described to regulate mouse 2-cell embryo development and 2C-like cell transcription *in vivo* and *in vitro* (Kigami et al., 2003; Peaston et al., 2004; Percharde et al., 2018; Svoboda et al., 2004). Although human LINEs and SINEs (long and short interspersed nuclear elements), as well as DNA transposons were detected at similar levels in both

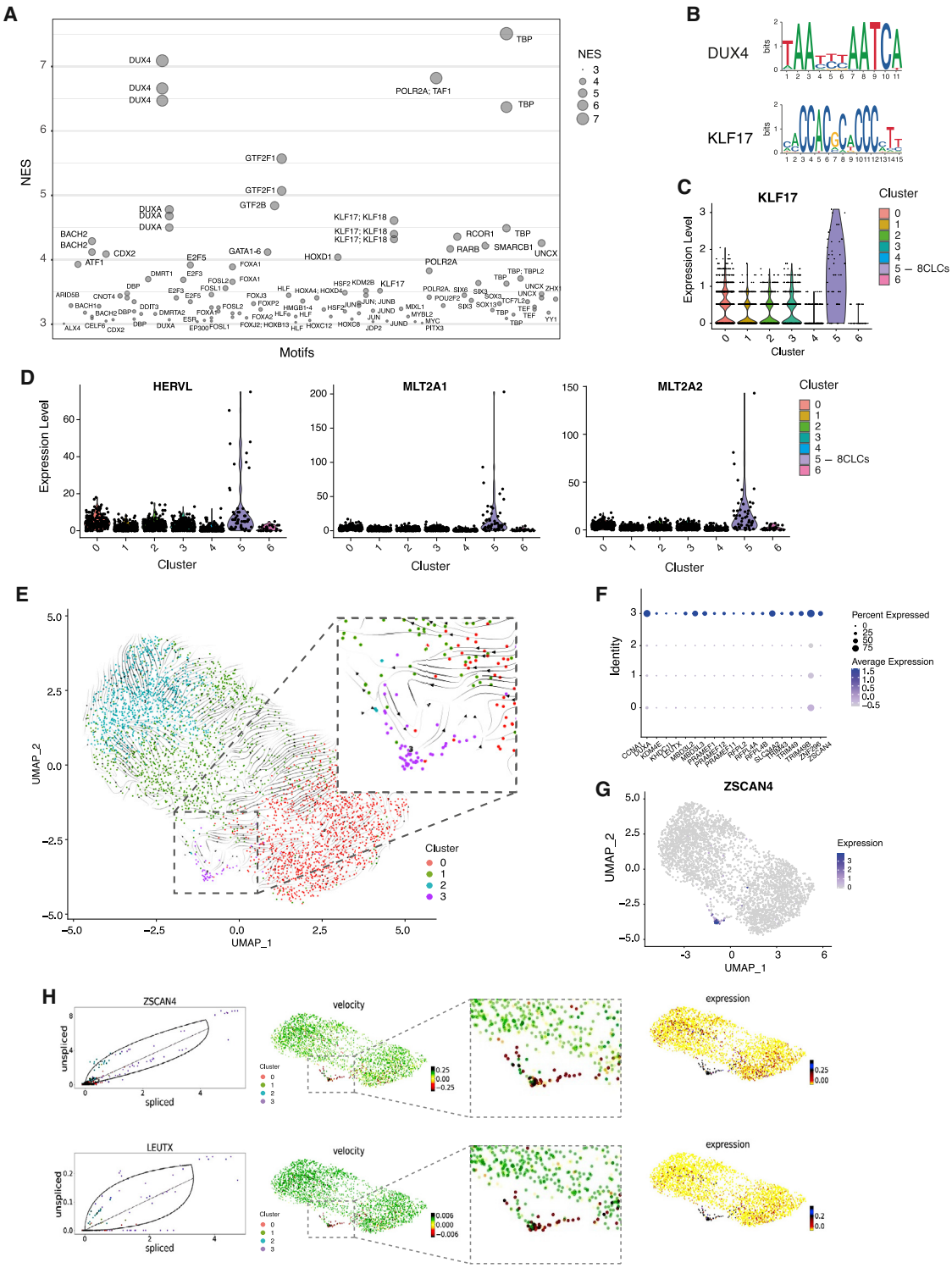

Figure 3. TF motifs and transposon expression in 8CLCs

(A) TF motifs identified around transcriptional start sites (TSS ± 10 kb) of the top 200 8CLCs signature genes using standard parameters in RcisTarget. NES, normalized enrichment score.

(B) DUX4- and KLF17-binding motifs as identified in (A) are shown.

(C) Violin plots of normalized, scaled *KLF17* expression in clustered naive human ESCs.

(D) Raw reads of transposable elements in clustered naive ESCs derived from single-cell RNA-seq data.

(legend continued on next page)

8CLCs and naive hESCs by bulk analysis, there was a trend for higher LTR element expression in 8CLCs (Figure S2G). We thus further analyzed LTR sub-families and found slightly higher levels of *LTR-ERVL* and *LTR-ERVK*, but not other LTRs, in 8C-like cells (Figure S2H). Remarkably, specific upregulation of *HERVL, MLT2A1*, and *MLT2A2* transcripts was detectable in some 8CLCs (cluster 5) but not in naive hESCs (Figure 3D). *MLT2A1, MLT2A2*, and *HERVL* are the most strongly upregulated repeats in the 8-cell human embryo *in vivo* and gain chromatin accessibility specifically during human ZGA (Liu et al., 2019). This shows that conserved ZGA-specific transposable elements are activated in some 8CLCs *in vitro*, similar to their upregulation in the embryo *in vivo*.

We next explored the gene expression dynamics in naive hESCs and 8CLCs. We used single-cell RNA velocity to compare immature with mature mRNA species and predict future RNA expression patterns and the direction of cell-fate transitions (Figure 3E). These analyses suggest bi-directional transitions from naive ESCs to 8CLCs and from 8CLCs toward the naive state (see arrows indicating direction of RNA velocity in cluster 3 cells, Figures 3E and 3F). This bi-directionality was also detectable in ZGA markers, such as *ZSCAN4* and *LEUTX*, which displayed an increase in RNA velocity in 8CLCs (higher unspliced to spliced ratio), corresponding to their upregulation, as well as a decrease, and hence downregulation, from 8CLCs toward the naive hESC state (Figures 3H and S3A). These data suggest dynamic gene expression changes and transitions of 8CLCs to and from naive hESCs, pointing toward a cycling nature of 8CLCs, similar to mouse 2CLCs.

8CLCs are marked by TPRX1 protein expression

We next wanted to define protein markers that can be used to identify 8CLCs *in vitro*. Although many genes are upregulated in 8CLCs (Figure S3B), we identified specifically one protein that is highly expressed in 8CLCs in culture, TPRX1 (Figure 4A). *TPRX1* (tetrapeptide repeat homeobox 1) is a protein coding gene of the paired (PRD)-like homeobox gene family of transcription factors that has been previously implicated in ZGA-like transcription; its biological role, however, is unknown (Madissoon et al., 2016; Maeso et al., 2016). Although TPRX1-positive cells were detected among naive HNES1 cells in culture, no primed H9 PSCs stained positive for the marker, and EpiLCs also appeared negative for TPRX1 (Figures 4A and S3C). TPRX1-expressing cells were found among reprogrammed naive H9 PSCs (WA09-NK2) and human fibroblast-derived naive iPSCs (FiPSCs) of non-embryonic origin, both grown under t2iLGö conditions (Takashima et al., 2014), as well as HNES1 cells grown in 4iLA and 5iLA (Theunissen et al., 2014, 2016) (Figure S3D). Analysis of stemness markers revealed that TPRX1-positive 8CLCs show reduced levels of the pluripotency marker SOX2, both at the transcriptional (Figure S3E) as well as protein level (Figures 4B, S3F, and S3G). We further analyzed DNA methylation levels and found that TPRX1+ cells have similar methyl CpG (mCpG) but increased 5-hydroxymethyl cytosine (5hmC) levels as compared with naive hESCs (Figures S3H–S3J). Moreover, some TPRX1-positive cells also display high levels of the DUX4 target gene H3.X/Y, both at the single-cell RNA level (Figure S3B), as well as at the protein level via immunofluorescence (Figure 4C). These results show that TRPX1, together with the histone-variant protein H3.X/Y, can be used to identify 8CLCs among naive human PSCs in culture.

Next, we wanted to see if 8CLC formation could be modified in culture. Since our motif analysis identified DUX4-binding sites enriched in 8CLC signature genes, we asked if *DUX4* overexpression would alter 8CLC abundance and hence introduce a codon-adapted version of the TF into naive hESCs (Jagannathan et al., 2016). Overexpression of *DUX4* did not only substantially increase transcription of ZGA marker genes, such as *LEUTX*, *ZSCAN4*, *TPRX1*, and *TRIM43* (Figure 4D), but also increased the number of TPRX1-positive, lower SOX2-expressing 8CLCs among naive hESCs in culture up to 20-fold (Figures 4E and S4A–S4C). Similar to wild-type 8CLCs, TPRX1+ cells generated via *DUX4* overexpression also harbor higher 5hmC levels (Figures S4D and S4E), some of which were also positive for H3.X/Y (Figure S4F), and notably, were actively dividing (Figure S4G). Additionally, induction of *DUX4* and subsequent withdrawal of transgene expression led to consequential downregulation of ZGA genes after the initial upregulation (Figure S4H), thus indicating that ZGA-like transcription is likely reversible and transient in naive hESCs. We characterized the exogenous *DUX4* (*DUX4-CA*)-expressing cells in more detail, transcriptionally and epigenetically. Although we could not reliably detect endogenous *DUX4* due to its low expression levels, we identified *DUX4-CA* as an additional marker of 8CLCs in our data (Figures S4I–S4K). Using single-cell multi-omics (combined scRNA-seq and scATAC-seq) we also sorted these cells computationally (based on their transcriptional signature) and have thus been able to generate chromatin accessibility profiles of 8CLCs, where we observed increased accessibility at sites proximal to ZGA markers, such as *ZSCAN4* and *RFPL4A*, as compared with naive hESCs (Figure S4L). This increased accessibility is also seen in 4- or 8-cell embryos prior to and around the time of genome activation (Figure S4L)—indicating that chromatin opening might precede transcription, as previously suggested in human embryos (Liu et al., 2019; Wu et al., 2018). These data illustrate that epigenetic and transcriptional ZGA-like transitions can be observed in 8CLCs *in vitro*.

In addition, we tested a recently reported spliceosome inhibitor, Pladienolide B, which has been shown to increase ZGA-like transcription and developmental potency in mouse stem cells (Shen et al., 2021). We observed a strong, dosage-dependent upregulation of ZGA genes, such as *ZSCAN4* and *H3.Y* in human ESCs, pointing toward a conserved role of spliceosome regulation in totipotency (Figure 4F). These results highlight that both ZGA-like transcription and *in vitro* 8CLC formation can be increased through genetic interference, such as *DUX4*

(E–G) (E) RNA velocity in naive hESCs and 8CLCs; cluster 3 represents 8CLCs, see also (F) ZGA marker and (G) *ZSCAN4* expression in clustered hESCs and 8CLCs.

(H) RNA velocity analysis of ZGA markers, such as *ZSCAN4* and *LEUTX*, in 8CLCs and naive hESCs. Left: steady-state ratio (black diagonal line), overall dynamics (black curve), and ratio of unspliced versus spliced mRNA in single cells, colored according to their cluster identity; middle: RNA velocity of marker genes; right: expression levels of markers.

CellPress
OPEN ACCESS

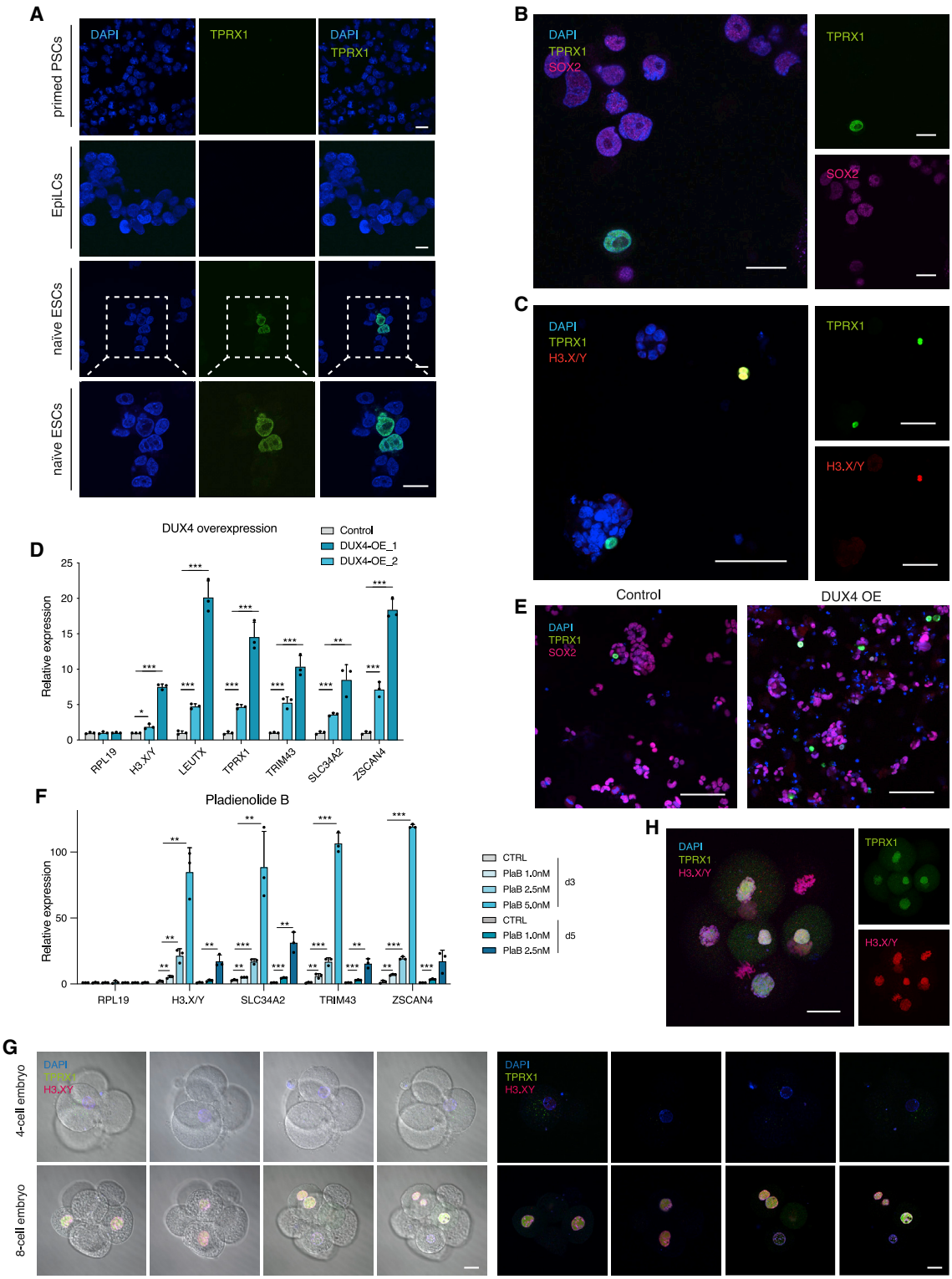

Figure 4. 8CLCs are marked by TPRX1 protein expression

(A) Immunofluorescence (IF) staining of cytospun naive ESCs, EpiLCs, and primed hPSCs for TPRX1. Scale bar, 15 μm.

(B) IF staining of TRPX1 and SOX2 in cytospun naive HNES1 cultured in PXGL. Scale bar, 20 μm.

(C) Representative images of H3.X/Y and TPRX1 stained HNES1 ESCs plated onto coverslips. Scale bar, 100 μm.

(D) Expression levels of ZGA marker genes assessed by RT-qPCR in two biological replicates of *DUX4* overexpressing HNES1 cells (*DUX4* OE) as compared with control cells (WT). Data are shown as mean ± SD (n = 3 technical replicates) of fold-change compared with control HNES1 and are representative of

(legend continued on next page)

overexpression, as well as pharmacological inhibition, such as Pladienolide B treatment, and can thus be used to study ZGA-like properties *in vitro*.

Finally, we tested if the identified 8CLC markers TPRX1 and H3.Y can also be detected in human pre-implantation-stage embryos not just transcriptionally (Figure S4M) but also as proteins. Remarkably, 8-cell human embryos stained strongly positive for TPRX1 and H3.Y at the time of human embryonic genome activation, but these markers were not detectable in 4-cell human embryos (Figure 4G). Interestingly, although TPRX1 was not present in blastomeres undergoing cell division, reassuringly the histone variant H3.Y showed strong association with prometa- and metaphase chromosomes in dividing cells (Figure 4H). These findings confirm the *in vitro* identified 8CLCs-specific proteins TPRX1 and H3.Y as markers of genome activation in human 8-cell embryos.

DISCUSSION

To analyze and manipulate the molecular events underlying genome activation, an *in vitro* model of human ZGA-like programs is needed. Such a system would not only have practical implications for our ability to study pre-implantation development functionally but would also improve our knowledge of human reproduction and health.

In this study, we report that human ZGA-like transcription, which occurs in the 8-cell embryo *in vivo*, can be found in a distinct population, approximately 1.6% of naive stem cells *in vitro*. We termed these cells "8-cell-like cells" (8CLCs). 8CLCs express ZGA markers, such as *ZSCAN4*, *LEUTX*, and *PRAMEFs*, and are characterized by an 8CLC-specific transcriptome signature, which further includes factors such as *DPPA3*, *H3.Y*, and *KLF17*. Our discovery of human 8CLCs as the first ZGA-stage cell population in a species other than mouse, with a comparable frequency (1%–5% of 2CLCs among mouse ESCs), suggests that this rare transcription event may be an intrinsic property of pluripotent stem cells rather than a randomly emerging one. The activation of transposable elements in 8CLCs strikingly similar to human 8-cell embryos also points toward conserved transcriptional networks in stem cells and embryos—akin to other repeat-element-driven cell states that have been reported (Grow et al., 2015; Pontis et al., 2019; Wang et al., 2014). As 8CLCs specifically activate transposable elements, such as *MLT2A1* and *MLT2A2*, which both harbor DUX4-binding sites, it will be important to assess their functional role in 8CLC formation and ZGA-like transcription *in vitro*.

We further identified TPRX1 as the first 8CLC marker protein that allows monitoring of ZGA-like transcription in cells *in vitro* as well as in 8-cell human embryos. *TPRX1* is itself an ETCHbox gene (eutherian-specific homeobox genes, which also include *LEUTX*, *ARGFX*, and *DPRX*) and has been found in human pre-implantation embryos transcriptionally (Jouhilahti et al., 2016; Maeso et al., 2016). Although *TPRX1* has been implicated in ZGA-like transcription before, its general biological function, as well as specifically during ZGA, still needs to be elucidated. Similarly, the second 8CLC marker that we described, H3.Y (Resnick et al., 2019), which is also expressed in the 8-cell human embryo and strongly upregulated upon *DUX4* induction, is a good candidate to study chromatin remodeling events involved in ZGA-like transcription *in vitro*. Importantly, the discovery that both *in vitro* identified 8CLC marker proteins TRPX1 and H3.Y are expressed in the nuclei of ZGA-stage 8-cell human embryos highlights their potential *in vivo* relevance and encourages further studies.

Interestingly, although 8CLCs upregulate some naive pluripotency markers, such as *DPPA3* and *KLF17*, they downregulate other stem cell markers, including SOX2, also at the protein level. It will be interesting to see if SOX2 downregulation occurs transiently and is a cause or consequence of 8CLC formation, and how compatible this reduction is with 8CLC survival and growth as compared with the pluripotency state in naive ESCs. It will be intriguing to see how these changes in transcription are reflected in cellular properties, such as differentiation potential. Moreover, it remains to be assessed whether 8CLCs possess increased developmental competence, similar to mouse 2CLCs, and would more readily contribute to extra-embryonic tissues in an embryo environment.

Altogether, we have discovered a unique cell state that enables the molecular characterization of ZGA-like transcription *in vitro*. The appearance, maintenance, and enrichment of 8CLCs will allow the study of genome activation in culture and make it amenable to genetic and pharmacological manipulation in a high-throughput way. Discoveries made from studying ZGA-like transcription *in vitro* may also provide important insights into the regulation of genome activation during human pre-implantation development and may have vital consequences for reproduction, health, and technology.

Limitations

Although 8CLCs will be useful to characterize human genome activation in a non-invasive, accessible, and systematic way *in vitro*, the validation of findings still depends on work in human embryos. Furthermore, although ZGA-like marker expression in 8CLCs and 8-cell blastomeres is highly similar, these two cell states expectedly differ as well. This is most likely due to differences in origin and maintenance (i.e., *in vitro* passaged cell lines as compared with directly fertilization-derived embryos), as well

three independent experiments. p value *p < 0.05, **p < 0.01, ***p < 0.001, absence of stars (ns, non-significant): p value > 0.05; unpaired, two-tailed Student's t test.

(E) IF staining of TPRX1 and SOX2 in *DUX4* overexpressing naive HNES1 and control cells in PXGL plated onto coverslips. Scale bar, 100 μm.

(F) ZGA marker gene expression measured by RT-qPCR in Pladienolide B (PlaB 1.0–5.0 nM, 3–5 days) and vehicle-treated control cells. Data are shown as mean ± SD (n = 3 technical replicates) of fold-change compared with control and are representative of three independent experiments. p value *p < 0.05, **p < 0.01, ***p < 0.001, absence of stars (ns, non-significant): p value > 0.05; unpaired, two-tailed Student's t test.

(G) Composite images of brightfield and immunofluorescent channels of TPRX1- and H3.X/Y-stained human pre-implantation embryos at the 4-cell and 8-cell stage. Four single optical sections are depicted of one representative 4-cell and 8-cell embryo, respectively. A total of two 4-cell and nine 8-cell-stage embryos were imaged. Scale bar, 25 μm.

(H) Immunofluorescence image of dividing human 8-cell-stage blastomeres stained for TPRX1 and H3.X/Y. A maximum intensity projection of a z stack of 172 individual optical sections of one embryo is shown. Scale bar, 25 μm.

as developmental potential (the ability to differentiate in tissue culture as compared with the capacity to generate a fully grown organism) of the two cell types. Moreover, although the genome was originally activated in human 8-cell embryos, 8CLCs have already undergone ZGA and are re-establishing ZGA-like programs *in vitro*.

Although most clustered 8CLCs are characterized by a defined transcriptional signature, certain markers are expressed to varying degrees in individual cells (Figure 1E). *ZSCAN4*, for example, is upregulated in most 8CLCs (see Figure S1G), whereas other markers, such as *TPRX1* or *DUXA*, are less broadly expressed (Figure S3B). The same is true for the upregulation of repeat elements. Transposable elements, such as *MLT2A1*, are highly expressed in some but not all 8CLCs (Figure 3D). Similarly, sequentially expressed or partly overlapping markers, such as *Mervl* and *Zscan4*, have also been previously reported in mouse 2CLCs. Exploring the heterogeneity of 8CLCs will be important to further understand intermediate states and the cellular mechanism underlying the formation of these transcriptional programs in culture.

Relatedly, the stability of 8CLCs requires further assessment and comparison with the mouse system, where 2CLCs have been reported to transiently cycle into and out of a ZGA-like state. Although we did not observe any changes in 8CLC percentage over time (>25 passages), we noticed that the upregulation of ZGA markers upon *DUX4* induction was only transient and reversible upon withdrawal. These results, together with the dynamic properties of 8CLCs in the RNA velocity analysis, point toward a cycling nature of 8CLCs in culture. More thorough experimental assessment of the stability of 8CLCs (i.e., stable, metastable, or transient) and their ability to revert back to the naive state (as well as their conversion rate) will be required to answer such questions definitely.

To utilize 8CLCs to their full potential, some technical hurdles still need to be overcome. For example, to isolate this subpopulation of cells for downstream applications that are not single-cell based, the identification of surface markers or the generation of endogenous reporter lines, similar to mouse 2CLC reporters, will be required. Also, enrichment of 8CLCs through adapted media compositions or altered culture conditions might allow increasing the numbers to obtain sufficient material for larger-scale experiments. Once isolation of 8CLCs can be done more easily, analyses of cell cycle and growth rates might help investigate origin and fate of 8CLCs in culture.

STAR★METHODS

Detailed methods are provided in the online version of this paper and include the following:

- KEY RESOURCES TABLE
- RESOURCE AVAILABILITY
  - Lead contact
  - Materials availability
  - Data and code availability
- EXPERIMENTAL MODEL AND SUBJECT DETAILS
  - Cell lines
  - Human embryos
- METHOD DETAILS
  - Pluripotent stem cell culture
  - *DUX4* overexpression in naive ESCs
  - Immunofluorescence staining and imaging of human PSCs
  - Thawing, immunohistochemistry staining, and imaging of human embryos
  - Quantitative reverse transcription PCR (qRT-PCR)
  - 10X Single-cell RNA-seq library preparation
  - 10X Single-cell Multiome library preparation
  - Single-cell RNA-seq data analysis
  - Transposable element analysis
  - Motif analysis
  - RNA velocity analysis
  - scATAC-seq data analysis
- QUANTIFICATION AND STATISTICAL ANALYSIS
  - Statistics and reproducibility

SUPPLEMENTAL INFORMATION

Supplemental information can be found online at https://doi.org/10.1016/j.stem.2022.01.014.

ACKNOWLEDGMENTS

We thank all members of the W.R. laboratory for helpful discussions and the Peter Rugg-Gunn laboratory for sharing reagents and stem cell expertise. We would also like to thank Christel Krueger and Simon Andrews for bioinformatics support, Simon Walker for imaging support, and the members of the flow cytometry and the sequencing facility at the Babraham Institute for assistance. We would like to thank Katarzyna Kania and the CRUK sequencing facility for single-cell sequencing support. We thank Austin Smith for providing stem cell lines. We would also like to acknowledge and thank the staff and patients at the assisted conception units at BMI Chelsfield Park and Leeds Fertility Hospitals. J.T.-S. is supported by an EMBO Fellowship (ALTF 355-2019) and a Charles and Katharine Darwin Research Fellowship at Darwin College. S.L. was supported by the Donald Higham Fund at Peterhouse College. J.N. is supported by the University of Cambridge and BBSRC (BB/T007044/1). R.A. is supported by the Wellcome for a Collaborative Award in Science (220379/Z/20/Z). Research in W.R.'s lab is supported by the BBSRC (BBS/E/B/000C0422) and the Wellcome Trust Investigator award (210754/Z/18/Z).

AUTHOR CONTRIBUTIONS

Conceptualization, J.T.-S. and W.R.; investigation, J.T.-S. with assistance from M.R., F.S., S.L., and J.N.; methodology, J.T.-S., M.R., F.S., and S.L.; formal analysis, J.T.-S., F.S., S.L., R.A., and F.K.; supervision, J.T.-S. and W.R.; writing – original draft, J.T.-S. and W.R.; writing – review and editing, all authors; funding acquisition, J.T.-S., J.N., and W.R.

DECLARATION OF INTERESTS

W.R. is a consultant and shareholder of Cambridge Epigenetix. All other authors declare no competing interests.

Received: June 18, 2021
Revised: October 26, 2021
Accepted: January 28, 2022
Published: February 24, 2022

REFERENCES

Aibar, S., González-Blas, C.B., Moerman, T., Huynh-Thu, V.A., Imrichova, H., Hulselmans, G., Rambow, F., Marine, J.C., Geurts, P., Aerts, J., et al. (2017). SCENIC: single-cell regulatory network inference and clustering. Nat. Methods *14*, 1083–1086.

Alda-Catalinas, C., Bredikhin, D., Hernando-Herraez, I., Santos, F., Kubinyecz, O., Eckersley-Maslin, M.A., Stegle, O., and Reik, W. (2020). A single-cell transcriptomics CRISPR-activation screen identifies epigenetic regulators of the zygotic genome activation program. Cell Syst. *11*, 25–41.e9.

Aoki, F., Worrad, D.M., and Schultz, R.M. (1997). Regulation of transcriptional activity during the first and second cell cycles in the preimplantation mouse embryo. Dev. Biol. *181*, 296–307.

Asami, M., Lam, B.Y.H., Ma, M.K., Rainbow, K., Braun, S., VerMilyea, M.D., Yeo, G.S.H., and Perry, A.C.F. (2021). Human embryonic genome activation initiates at the one-cell stage. Cell Stem Cell.

Bentsen, M., Goymann, P., Schultheis, H., Klee, K., Petrova, A., Wiegandt, R., Fust, A., Preussner, J., Kuenne, C., Braun, T., et al. (2020). ATAC-seq footprinting unravels kinetics of transcription factor binding during zygotic genome activation. Nat. Commun. *11*, 4267.

Bergen, V., Lange, M., Peidli, S., Wolf, F.A., and Theis, F.J. (2020). Generalizing RNA velocity to transient cell states through dynamical modeling. Nat. Biotechnol. *38*, 1408–1414.

Blakeley, P., Fogarty, N.M., del Valle, I., Wamaitha, S.E., Hu, T.X., Elder, K., Snell, P., Christie, L., Robson, P., and Niakan, K.K. (2015). Defining the three cell lineages of the human blastocyst by single-cell RNA-seq. Development *142*, 3151–3165.

Braude, P., Bolton, V., and Moore, S. (1988). Human gene expression first occurs between the four- and eight-cell stages of preimplantation development. Nature *332*, 459–461.

Bredenkamp, N., Yang, J., Clarke, J., Stirparo, G.G., von Meyenn, F., Dietmann, S., Baker, D., Drummond, R., Ren, Y., Li, D., et al. (2019). Wnt inhibition facilitates RNA-mediated reprogramming of human somatic cells to naive pluripotency. Stem Cell Rep. *13*, 1083–1098.

De Iaco, A., Planet, E., Coluccio, A., Verp, S., Duc, J., and Trono, D. (2017). DUX-family transcription factors regulate zygotic genome activation in placental mammals. Nat. Genet. *49*, 941–945.

Eckersley-Maslin, M.A., Svensson, V., Krueger, C., Stubbs, T.M., Giehr, P., Krueger, F., Miragaia, R.J., Kyriakopoulos, C., Berrens, R.V., Milagre, I., et al. (2016). MERVL/Zscan4 network activation results in transient genome-wide DNA demethylation of mESCs. Cell Rep. *17*, 179–192.

Evans, M.J., and Kaufman, M.H. (1981). Establishment in culture of pluripotential cells from mouse embryos. Nature *292*, 154–156.

Falco, G., Lee, S.L., Stanghellini, I., Bassey, U.C., Hamatani, T., and Ko, M.S. (2007). Zscan4: a novel gene expressed exclusively in late 2-cell embryos and embryonic stem cells. Dev. Biol. *307*, 539–550.

Granja, J.M., Corces, M.R., Pierce, S.E., Bagdatli, S.T., Choudhry, H., Chang, H.Y., and Greenleaf, W.J. (2021). ArchR is a scalable software package for integrative single-cell chromatin accessibility analysis. Nat. Genet. *53*, 403–411.

Grow, E.J., Flynn, R.A., Chavez, S.L., Bayless, N.L., Wossidlo, M., Wesche, D.J., Martin, L., Ware, C.B., Blish, C.A., Chang, H.Y., et al. (2015). Intrinsic retroviral reactivation in human preimplantation embryos and pluripotent cells. Nature *522*, 221–225.

Guo, G., von Meyenn, F., Rostovskaya, M., Clarke, J., Dietmann, S., Baker, D., Sahakyan, A., Myers, S., Bertone, P., Reik, W., et al. (2017). Epigenetic resetting of human pluripotency. Development *144*, 2748–2763.

Guo, G., von Meyenn, F., Santos, F., Chen, Y., Reik, W., Bertone, P., Smith, A., and Nichols, J. (2016). Naive pluripotent stem cells derived directly from isolated cells of the human inner cell mass. Stem Cell Rep. *6*, 437–446.

Guo, G., Yang, J., Nichols, J., Hall, J.S., Eyres, I., Mansfield, W., and Smith, A. (2009). Klf4 reverts developmentally programmed restriction of ground state pluripotency. Development *136*, 1063–1069.

Hao, Y., Hao, S., Andersen-Nissen, E., Mauck, W.M.3rd, Zheng, S., Butler, A., Lee, M.J., Wilk, A.J., Darby, C., Zager, M., et al. (2021). Integrated analysis of multimodal single-cell data. Cell.

Hendrickson, P.G., Doráis, J.A., Grow, E.J., Whiddon, J.L., Lim, J.W., Wike, C.L., Weaver, B.D., Pflueger, C., Emery, B.R., Wilcox, A.L., et al. (2017). Conserved roles of mouse DUX and human DUX4 in activating cleavage-stage genes and MERVL/HERVL retrotransposons. Nat. Genet. *49*, 925–934.

Huang, K., Maruyama, T., and Fan, G. (2014). The naive state of human pluripotent stem cells: a synthesis of stem cell and preimplantation embryo transcriptome analyses. Cell Stem Cell *15*, 410–415.

Huang, Y., Kim, J.K., Do, D.V., Lee, C., Penfold, C.A., Zylicz, J.J., Marioni, J.C., Hackett, J.A., and Surani, M.A. (2017). Stella modulates transcriptional and endogenous retrovirus programs during maternal-to-zygotic transition. Elife *6*, e22345.

Ishiuchi, T., Enriquez-Gasca, R., Mizutani, E., Bošković, A., Ziegler-Birling, C., Rodriguez-Terrones, D., Wakayama, T., Vaquerizas, J.M., and Torres-Padilla, M.E. (2015). Early embryonic-like cells are induced by downregulating replication-dependent chromatin assembly. Nat. Struct. Mol. Biol. *22*, 662–671.

Jagannathan, S., Shadle, S.C., Resnick, R., Snider, L., Tawil, R.N., van der Maarel, S.M., Bradley, R.K., and Tapscott, S.J. (2016). Model systems of DUX4 expression recapitulate the transcriptional profile of FSHD cells. Hum. Mol. Genet. *25*, 4419–4431.

Jiang, S., Williams, K., Kong, X., Zeng, W., Nguyen, N.V., Ma, X., Tawil, R., Yokomori, K., and Mortazavi, A. (2020). Single-nucleus RNA-seq identifies divergent populations of FSHD2 myotube nuclei. PLOS Genet. *16*, e1008754.

Jouhilahti, E.M., Madissoon, E., Vesterlund, L., Töhönen, V., Krjutškov, K., Plaza Reyes, A., Petropoulos, S., Månsson, R., Linnarsson, S., Bürglin, T., et al. (2016). The human PRD-like homeobox gene LEUTX has a central role in embryo genome activation. Development *143*, 3459–3469.

Kigami, D., Minami, N., Takayama, H., and Imai, H. (2003). MuERV-L is one of the earliest transcribed genes in mouse one-cell embryos. Biol. Reprod. *68*, 651–654.

La Manno, G., Soldatov, R., Zeisel, A., Braun, E., Hochgerner, H., Petukhov, V., Lidschreiber, K., Kastriti, M.E., Lönnerberg, P., Furlan, A., et al. (2018). RNA velocity of single cells. Nature *560*, 494–498.

Langmead, B., Trapnell, C., Pop, M., and Salzberg, S.L. (2009). Ultrafast and memory-efficient alignment of short DNA sequences to the human genome. Genome Biology *10*, R25.

Latham, K.E., and Schultz, R.M. (2001). Embryonic genome activation. Front. Biosci. *6*, D748–D759.

Lee, M.T., Bonneau, A.R., and Giraldez, A.J. (2014). Zygotic genome activation during the maternal-to-zygotic transition. Annu. Rev. Cell Dev. Biol. *30*, 581–613.

Li, H., Handsaker, B., Wysoker, A., Fennell, T., Ruan, J., Homer, N., Marth, G., Abecasis, G., and Durbin, R.; Genome Project Data Processing, S. (2009). The Sequence Alignment/Map format and SAMtools. Bioinformatics *25*, 2078–2079.

Liu, L., Leng, L., Liu, C., Lu, C., Yuan, Y., Wu, L., Gong, F., Zhang, S., Wei, X., Wang, M., et al. (2019). An integrated chromatin accessibility and transcriptome landscape of human pre-implantation embryos. Nat. Commun. *10*, 364.

Macfarlan, T.S., Gifford, W.D., Driscoll, S., Lettieri, K., Rowe, H.M., Bonanomi, D., Firth, A., Singer, O., Trono, D., and Pfaff, S.L. (2012). Embryonic stem cell potency fluctuates with endogenous retrovirus activity. Nature *487*, 57–63.

Madissoon, E., Jouhilahti, E.M., Vesterlund, L., Töhönen, V., Krjutškov, K., Petropoulos, S., Einarsdottir, E., Linnarsson, S., Lanner, F., Månsson, R., et al. (2016). Characterization and target genes of nine human PRD-like homeobox domain genes expressed exclusively in early embryos. Sci. Rep. *6*, 28995.

Maeso, I., Dunwell, T.L., Wyatt, C.D., Marlétaz, F., Vető, B., Bernal, J.A., Quah, S., Irimia, M., and Holland, P.W. (2016). Evolutionary origin and functional divergence of totipotent cell homeobox genes in eutherian mammals. BMC Biol. *14*, 45.

Messmer, T., von Meyenn, F., Savino, A., Santos, F., Mohammed, H., Lun, A.T.L., Marioni, J.C., and Reik, W. (2019). Transcriptional heterogeneity in naive and primed human pluripotent stem cells at single-cell resolution. Cell Rep. *26*, 815–824.e4.

Nakamura, T., Okamoto, I., Sasaki, K., Yabuta, Y., Iwatani, C., Tsuchiya, H., Seita, Y., Nakamura, S., Yamamoto, T., and Saitou, M. (2016). A developmental coordinate of pluripotency among mice, monkeys and humans. Nature *537*, 57–62.

Niakan, K.K., Han, J., Pedersen, R.A., Simon, C., and Pera, R.A. (2012). Human pre-implantation embryo development. Development *139*, 829–841.

Peaston, A.E., Evsikov, A.V., Graber, J.H., de Vries, W.N., Holbrook, A.E., Solter, D., and Knowles, B.B. (2004). Retrotransposons regulate host genes in mouse oocytes and preimplantation embryos. Dev. Cell *7*, 597–606.

Percharde, M., Lin, C.J., Yin, Y., Guan, J., Peixoto, G.A., Bulut-Karslioglu, A., Biechele, S., Huang, B., Shen, X., and Ramalho-Santos, M. (2018). A LINE1-nucleolin partnership regulates early development and ESC identity. Cell *174*, 391–405, e319.

Petropoulos, S., Edsgärd, D., Reinius, B., Deng, Q., Panula, S.P., Codeluppi, S., Plaza Reyes, A., Linnarsson, S., Sandberg, R., and anner, F. (2016). Single-cell RNA-Seq reveals lineage and X chromosome dynamics in human preimplantation embryos. Cell *165*, 1012–1026.

Pontis, J., Planet, E., Offner, S., Turelli, P., Duc, J., Coudray, A., Theunissen, T.W., Jaenisch, R., and Trono, D. (2019). Hominoid-specific transposable elements and KZFPs facilitate human embryonic genome activation and control transcription in naive human ESCs. Cell Stem Cell *24*, 724–735.e5.

Resnick, R., Wong, C.J., Hamm, D.C., Bennett, S.R., Skene, P.J., Hake, S.B., Henikoff, S., van der Maarel, S.M., and Tapscott, S.J. (2019). DUX4-induced histone variants H3.X and H3.Y Mark DUX4 target genes for expression. Cell Rep. *29*, 1812–1820.e5.

Rodriguez-Terrones, D., Gaume, X., Ishiuchi, T., Weiss, A., Kopp, A., Kruse, K., Penning, A., Vaquerizas, J.M., Brino, L., and Torres-Padilla, M.E. (2018). A molecular roadmap for the emergence of early-embryonic-like cells in culture. Nat. Genet. *50*, 106–119.

Roode, M., Blair, K., Snell, P., Elder, K., Marchant, S., Smith, A., and Nichols, J. (2012). Human hypoblast formation is not dependent on FGF signalling. Dev. Biol. *361*, 358–363.

Rostovskaya, M., Stirparo, G.G., and Smith, A. (2019). Capacitation of human naive pluripotent stem cells for multi-lineage differentiation. Development *146*.

Shen, H., Yang, M., Li, S., Zhang, J., Peng, B., Wang, C., Chang, Z., Ong, J., and Du, P. (2021). Mouse totipotent stem cells captured and maintained through spliceosomal repression. Cell *184*, 2843–2859.e20.

Stirparo, G.G., Boroviak, T., Guo, G., Nichols, J., Smith, A., and Bertone, P. (2018). Integrated analysis of single-cell embryo data yields a unified transcriptome signature for the human pre-implantation epiblast. Development *145*, dev158501.

Sumi, T., Oki, S., Kitajima, K., and Meno, C. (2013). Epiblast ground state is controlled by canonical Wnt/beta-catenin signaling in the postimplantation mouse embryo and epiblast stem cells. PLoS One *8*, e63378.

Svoboda, P., Stein, P., Anger, M., Bernstein, E., Hannon, G.J., and Schultz, R.M. (2004). RNAi and expression of retrotransposons MuERV-L and IAP in preimplantation mouse embryos. Dev. Biol. *269*, 276–285.

Takashima, Y., Guo, G., Loos, R., Nichols, J., Ficz, G., Krueger, F., Oxley, D., Santos, F., Clarke, J., Mansfield, W., et al. (2014). Resetting transcription factor control circuitry toward ground-state pluripotency in human. Cell *158*, 1254–1269.

Tarkowski, A.K. (1959). Experiments on the development of isolated blastomers of mouse eggs. Nature *184*, 1286–1287.

Theunissen, T.W., Friedli, M., He, Y., Planet, E., O'Neil, R.C., Markoulaki, S., Pontis, J., Wang, H., Iouranova, A., Imbeault, M., et al. (2016). Molecular criteria for defining the naive human pluripotent state. Cell Stem Cell *19*, 502–515.

Theunissen, T.W., Powell, B.E., Wang, H., Mitalipova, M., Faddah, D.A., Reddy, J., Fan, Z.P., Maetzel, D., Ganz, K., Shi, L., et al. (2014). Systematic identification of culture conditions for induction and maintenance of naive human pluripotency. Cell Stem Cell *15*, 524–526.

Thomson, J.A., Itskovitz-Eldor, J., Shapiro, S.S., Waknitz, M.A., Swiergiel, J.J., Marshall, V.S., and Jones, J.M. (1998). Embryonic stem cell lines derived from human blastocysts. Science *282*, 1145–1147.

Vassena, R., Boué, S., González-Roca, E., Aran, B., Auer, H., Veiga, A., and Izpisua Belmonte, J.C. (2011). Waves of early transcriptional activation and pluripotency program initiation during human preimplantation development. Development *138*, 3699–3709.

Wang, J., Xie, G., Singh, M., Ghanbarian, A.T., Raskó, T., Szvetnik, A., Cai, H., Besser, D., Prigione, A., Fuchs, N.V., et al. (2014). Primate-specific endogenous retrovirus-driven transcription defines naive-like stem cells. Nature *516*, 405–409.

Wu, J., Xu, J., Liu, B., Yao, G., Wang, P., Lin, Z., Huang, B., Wang, X., Li, T., Shi, S., et al. (2018). Chromatin analysis in human early development reveals epigenetic transition during ZGA. Nature *557*, 256–260.

Xue, Z., Huang, K., Cai, C., Cai, L., Jiang, C.Y., Feng, Y., Liu, Z., Zeng, Q., Cheng, L., Sun, Y.E., et al. (2013). Genetic programs in human and mouse early embryos revealed by single-cell RNA sequencing. Nature *500*, 593–597.

Yan, L., Yang, M., Guo, H., Yang, L., Wu, J., Li, R., Liu, P., Lian, Y., Zheng, X., Yan, J., et al. (2013). Single-cell RNA-Seq profiling of human preimplantation embryos and embryonic stem cells. Nat. Struct. Mol. Biol. *20*, 1131–1139.

Yao, Z., Snider, L., Balog, J., Lemmers, R.J., Van Der Maarel, S.M., Tawil, R., and Tapscott, S.J. (2014). DUX4-induced gene expression is the major molecular signature in FSHD skeletal muscle. Hum. Mol. Genet. *23*, 5342–5352.

Yoshihara, M., Kirjanov, I., Nykänen, S., Sokka, J., Weltner, J., Lundin, K., Gawriyski, L., Jouhilahti, E.-M., Varjosalo, M., Tervaniemi, M.H., et al. (2021). Transient DUX4 expression induces blastomere-like expression program that is marked by SLC34A2. bioRxiv, 2021.2008.2025.457357.

Zalzman, M., Falco, G., Sharova, L.V., Nishiyama, A., Thomas, M., Lee, S.L., Stagg, C.A., Hoang, H.G., Yang, H.T., Indig, F.E., et al. (2010). Zscan4 regulates telomere elongation and genomic stability in ES cells. Nature *464*, 858–863.

Zheng, G.X., Terry, J.M., Belgrader, P., Ryvkin, P., Bent, Z.W., Wilson, R., Ziraldo, S.B., Wheeler, T.D., McDermott, G.P., Zhu, J., et al. (2017). Massively parallel digital transcriptional profiling of single cells. Nature communications *8*, 14049.

STAR★METHODS

KEY RESOURCES TABLE

REAGENT or RESOURCE	SOURCE	IDENTIFIER
Antibodies		
Rabbit polyclonal anti-TPRX1 antibody	Sigma Aldrich	Cat#HPA044922; RRID: AB_10962509
Rat monoclonal anti-H3.X/Y antibody	Active Motif	Cat#61161; RRID: AB_2793533
Goat polyclonal anti-SOX2 antibody	R&D systems	Cat#AF2018; RRID: AB_355110
Mouse monoclonal mCpG antibody	This paper	Clone 3A7 B9C8
Rabbit polyclonal anti-5hmC antibody	Active Motif	Cat#39769; RRID: AB_10013602
Donkey anti-Rabbit IgG (H+L) secondary antibody, Alexa Fluor 488	Invitrogen	Cat#A-21206; RRID: AB_2535792
Goat anti-Rat IgG (H+L) scondary antibody, Alexa Fluor 568	Invitrogen	Cat#A-11077; RRID: AB_2534121
Donkey anti-Goat IgG (H+L) secondary antibody, Alexa Fluor 647	Invitrogen	Cat#A-21447; RRID: AB_2535864
Bacterial and virus strains		
One Shot™ Stbl3™ Chemically Competent E. coli	Invitrogen	Cat#C737303
Library Efficiency™ DH5α Competent Cells	Invitrogen	Cat#18263012
Chemicals, peptides, and recombinant proteins		
Neurobasal Medium	Thermo Fisher Scientific	Cat#11540566
DMEM/F12 Medium	Thermo Fisher Scientific	Cat#21103049
GlutaMax	Thermo Fisher Scientific	Cat#35050061
Non-Essential Amino Acids	Thermo Fisher Scientific	Cat#11140035
Penicillin-Streptomycin	Thermo Fisher Scientific	Cat#15140122
Sodium Pyruvate	Thermo Fisher Scientific	Cat#11360039
N2 Supplement	Thermo Fisher Scientific	Cat#17502048
B27 Supplement	Thermo Fisher Scientific	Cat#17504044
Essential 8 Medium	Thermo Fisher Scientific	Cat#A1517001
Geltrex LDEV-Free, hESC-Qualified, Reduced Growth Factor Basement Membrane Matrix	Thermo Fisher Scientific	Cat#A1413302
TrypLE Express Enzyme	Thermo Fisher Scientific	Cat#12605028
UltraPure 0.5M EDTA, pH 8.0	Thermo Fisher Scientific	Cat#15575020
Corning Matrigel Basement Membrane Matrix	Fisher Scientific	Cat#15575729
Recombinant human LIF	WT-MRC Cambridge Stem Cell Institute	N/A
Recombinant Activin A	WT-MRC Cambridge Stem Cell Institute	N/A
Recombinant FGF2	WT-MRC Cambridge Stem Cell Institute	N/A
CHIR99021 GSK3 inhibitor	WT-MRC Cambridge Stem Cell Institute	CAS: 252917-06-9
PD0325901 MEK inhibitor	WT-MRC Cambridge Stem Cell Institute	CAS: 391210-10-9
WH-4-023 Src Inhibitor	A Chemtek	Cat#0104-002013; CAS: 837422-57-8
IM-12 GSK3 inhibitor	Sigma-Aldrich	Cat#SML0084; CAS: 1129660-05-1
SB590885 B-Raf inhibitor	Sigma-Aldrich	Cat#SML0501; CAS: 405554-55-4
Y-27632 ROCK inhibitor	Millipore	Cat#688000; CAS: 146986-50-7
Gö6983 aPKC inhibitor	Tocris	Cat#2285; CAS: 133053-19-7
XAV939 Tankyrase inhibitor	Tocris	Cat#3748; CAS: 284028-89-3

(*Continued on next page*)

Continued

REAGENT or RESOURCE	SOURCE	IDENTIFIER
Pladienolide B spliceosome inhibitor	Tocris	Cat#6070; CAS: 445493-23-2
Critical commercial assays		
Chromium Single Cell 3′ Library & Gel Bead Kit v3	10x Genomics	PN-1000075
Chromium Chip B Kit	10x Genomics	PN-1000073
Chromium Next GEM Single Cell Multiome ATAC + Gene Expression Reagent bundle	10x Genomics	PN-1000283
Chromium Next GEM Chip J Single Cell Kit	10x Genomics	PN-1000234
Neon 100ul transfection kit	Thermo Fisher Scientific	Cat#MPK10096
Deposited data		
Raw and quantified sequencing data: 10X single-cell RNA-seq of human naïve ESCs	This paper	GEO: GSE178379; GSM5389327 https://www.ncbi.nlm.nih.gov/geo/query/acc.cgi?acc=GSM5389327
Raw and quantified sequencing data: 10X single-cell Multiome seq of wildtype human naïve ESCs	This paper	GEO: GSE178379; GSM5694433; GSM5694435; https://www.ncbi.nlm.nih.gov/geo/query/acc.cgi?acc=GSM5389327
Raw and quantified sequencing data: 10X single-cell Multiome seq of *DUX4* overexpressing human naïve ESCs	This paper	GEO: GSE178379; GSM5694434; GSM5694436; https://www.ncbi.nlm.nih.gov/geo/query/acc.cgi?acc=GSM5389327
Raw sequencing data: single cell RNA-seq data of human primed PSCs	Messmer et al. (2019)	ArrayExpress: E-MTAB-6819
Raw sequencing data: naïve hPSCs, primed hPSCs	Rostovskaya et al. (2019)	GEO: GSE123055
Raw sequencing data: *DUX4* overexpression in human primed PSCs	Hendrickson et al. (2017)	GEO: GSE85632
Raw sequencing data: *DUX4* overexpression in human myocytes	Jiang et al. (2020)	GEO: GSE143493
Raw sequencing data: *DUX4* upregulation in human FSHD patient myotubes	Yao et al. (2014)	GEO: GSE56787
Raw sequencing data: RNA-seq of human pre-implantation embryo cells	Yan et al. (2013)	GEO: GSE36552
Raw sequencing data: RNA-seq of human pre-implantation embryo cells	Xue et al. (2013)	GEO: GSE44183
Raw sequencing data: single cell RNA-seq data of human preimplantation stage embryos	Petropoulos et al. (2016)	ArrayExpress: E-MTAB-3929
Raw sequencing data: single celll ATAC-seq of human pre-implantation embryo cells	Liu et al. (2019)	SRA: SRP163205
Human reference genome NCBI build 38, GRCh38 human genome	Genome Reference Consortium	https://www.ncbi.nlm.nih.gov/assembly/GCF_000001405.26
Human repeat element annotation, GRCh37	RepeatMasker	http://www.repeatmasker.org
Experimental models: Cell lines		
Human: HNES1 ES cells	Guo et al. (2016)	https://hpscreg.eu/cell-line/CAMe001-A
Human: WA09/H9 primed PSCs	WiCell	https://hpscreg.eu/cell-line/WAe009-A
Human: WA09/H9 NK2 naive and primed PSCs	Austin Smith lab; Takashima et al. (2014)	N/A
Human: WA09/H9 FiPS naive and primed PSCs	Austin Smith lab; Takashima et al. (2014)	N/A
Oligonucleotides		
Primers for qRT-PCRs, see Table S4	This paper	Table S4
Recombinant DNA		
Plasmid: pPB_Tet3G_DUX4-CA_BFP	This paper	N/A
Plasmid: PBase	Guo et al. (2009)	N/A

(*Continued on next page*)

Continued

REAGENT or RESOURCE	SOURCE	IDENTIFIER
Software and algorithms		
CellRanger v3.1.0	(Zheng et al., 2017)	https://support.10xgenomics.com/single-cell-gene-expression/software/downloads/latest
SAMtools v1.11	Li et al. (2009)	http://samtools.sourceforge.net/
Bowtie2 v2.4.2	Langmead et al. (2009)	https://github.com/BenLangmead/bowtie2
R v1.4.1	N/A	https://www.r-project.org/
Seurat v4	Hao et al. (2021)	https://satijalab.org/seurat/
Velocyto v0.17	La Manno et al. (2018)	https://velocyto.org/velocyto.py
scVelo v0.2.4	Bergen et al. (2020)	https://scvelo.readthedocs.io
RcisTarget v1.10.0	Aibar et al. (2017)	https://bioconductor.org/packages/release/bioc/html/RcisTarget.html
ArchR v1.0.1	Granja et al. (2021)	https://www.archrproject.com
Fiji ImageJ v2.1.0/1.53c	Fiji	https://imagej.net/software/fiji/downloads
Volocity v6.3	Perkin Elmer/ formerly Improvision	http://www.perkinelmer.com/pages/020/cellularimaging/products/volocity.xhtml
Graphpad Prism v9.3.1	Graphpad Software	https://www.graphpad.com/prism
Other		
Repeat analysis	This paper	https://github.com/FelixKrueger/scRepeats
scATAC analysis	This paper	https://github.com/rargelaguet/DUX4_8CLC_hESCs

RESOURCE AVAILABILITY

Lead contact

Further information and requests for resources and reagents should be directed to and will be fulfilled by the lead contact, Wolf Reik (wolf.reik@babraham.ac.uk).

Materials availability

The plasmid generated in this study (pPB_Tet3G_DUX4-CA_BFP) is available from the lead contact, Wolf Reik (wolf.reik@babraham.ac.uk), upon request.

Data and code availability

- Single-cell RNA-seq and 10x Multiome data generated in this paper have been deposited at GEO and are publicly available as of the date of publication. Accession numbers are listed in the key resources table. This paper also analyses existing, publicly available data. These accession numbers for the datasets are listed in the key resources table.
- All original code has been deposited at GitHub and is publicly available as of the date of publication. Links are listed in the key resources table.
- Any additional information required to reanalyse the data reported in this paper is available from the lead contact upon request.

EXPERIMENTAL MODEL AND SUBJECT DETAILS

Cell lines

WA09/H9 (female) PSCs were obtained from WiCell, WA09/H9 NK2 and FiPSCs were kindly provided by Austin Smith (Takashima et al., 2014). HNES1 (male) were described previously (Guo et al., 2016). All PSCs were cultured in 5% O2, 5% CO2 at 37°C.

Human embryos

Cryopreserved 4-8 cell stage human embryos were left over from assisted conception programmes and kindly donated with informed consent to Human Fertilisation and Embryology Authority licence R0178, approval number 21/PR/1231. After thawing, the embryos were recovered, the zonae pellucidae was removed and the embryos were immediately fixed.

METHOD DETAILS

Pluripotent stem cell culture

Naïve stem cells were maintained on irradiated mouse embryonic fibroblast feeder cells (p2 DR4 expanded MEFs from WT-MRC Cambridge Stem Cell Institute) and were passaged every 2-3 days using TrypLE (Thermo Fisher Scientific, 12605028). ROCK inhibitor (10μM; Y-27632, 688000, Millipore) was added for 24h after passaging. Geltrex (hESC-qualified, Thermo Fisher Scientific, A1413302) was optionally added to the medium during re-plating on feeders (0.5μl per cm2 surface are) or without feeder cells (1.0μl per cm2).

Embryo-derived HNES1 naïve stem cells were cultured in PXGL culture conditions: N2B27 (1:1 DMEM/F12:Neurobasal, 0.5x N2 supplement, 0.5x B27 supplement, 1x nonessential amino acids, 2mM l-Glutamine, 1x Penicillin/Streptomycin (all from ThermoFisher Scientific), 0.1mM β-mercaptoethanol (Sigma-Aldrich), supplemented with 1μM PD0325901 (WT-MRC Cambridge Stem Cell Institute), 2μM Gö6983 (Tocris Bio-Techne, 2285), 2μM XAV939 (Tocris Bio-Techne, 3748) and 10ng/ mL human LIF (WT-MRC Cambridge Stem Cell Institute) (Guo et al., 2016; Bredenkamp et al., 2019).

For 5iLA media conditions, HNES1 were cultured in: N2B27 (see above), supplemented with 1μM PD0325901 (WT-MRC Cambridge Stem Cell Institute), 1μM IM-12 (Sigma-Aldrich), 0.5μM SB590885 (SigmaAldrich), 1μM WH-4-023 (A Chemtek), 10μM Y-27632 (Cell Guidance Systems), 50μg/ml bovine serum albumin (ThermoFisher Scientific), 0.5% KnockOut Serum Replacement (KSR; ThermoFisher Scientific), 20ng/ml Activin A (WT-MRC Cambridge Stem Cell Institute) and 10ng/mL human LIF (WT-MRC Cambridge Stem Cell Institute). 4iLA media was the same as 5iLA but with the omission of 1μM IM-12, the GSK3i (Theunissen et al., 2016; Theunissen et al., 2014).

WA09-NK2 H9 and fibroblast derived FiPSCs naïve stem cells were maintained in t2iLGö: N2B27 (see above), supplemented with 1μM PD0325901 (WT-MRC Cambridge Stem Cell Institute), 2μM Gö6983 (Tocris Bio-Techne, 2285), 1μM CHIR99021 (WT-MRC Cambridge Stem Cell Institute) and 10ng/mL human LIF (WT-MRC Cambridge Stem Cell Institute) (Takashima et al., 2014).

Primed WA09-NK2 PSCs were maintained in Essential 8 (E8) medium (Thermo Fisher Scientific A1517001) on Matrigel (Corning™ Matrigel™ Basement Membrane Matrix, Thermo Fisher Scientific 15575729). Primed stem cells were cultured in a humidified incubator at 5% O2, 5% CO2 and 37°C. They were passaged every 2-3 days using EDTA (UltraPure 0.5M EDTA, pH 8.0, 15575020, Thermo Fisher Scientific). ROCK inhibitor (10μM; Y-27632, 688000, Millipore) was optionally added for 24h after passaging or thawing.

DUX4 overexpression in naive ESCs

A codon adapted version of human DUX4 (pCW57.1-DUX4-CA, Addgene plasmid #99281) was cloned into an inducible, BFP containing vector harbouring IR (inverted repeats) compatible with PBase (PiggyBac transposase). For inducible DUX4 expression, 1x10^6 HNES1 cells were plated onto Geltrex with ROCK inhibitor for 24h-48h, and electroporated using the NEON Transfection System and 100μl kit (Thermo Fisher Scientific, MPK10096) with 3ug PBase plasmid and 3ug vector. The conditions used for the NEON electroporation were the following: 1150V, 30ms pulse width, 2 pulses. Stable BFP expressing cells were sorted using FACS after >72h and expanded. DUX4 expression was induced by Doxycycline for 2-4h (2μg/ mL).

Immunofluorescence staining and imaging of human PSCs

Naïve and primed human PSCs were plated on coverslips (on Geltrex or Matrigel) or cytospun onto poly-L-lysine coated glass slides (300rpm, 3min), washed with 1x PBS and fixed with 2% PFA in PBS for 30min at room temperature (RT). They were then permeabilized with 0.5% Triton X-100 in PBS for 1 hour at RT, blocked with 1% BSA, 0.05% Tween20 in PBS for 1 hour at RT, and incubated with primary antibody diluted in blocking solution for 1 hour at RT or o/n at 4°C. After washing in blocking solution for 30 min at RT, secondary antibodies were added for 1h at room temperature and cells were washed again. DNA was counterstained with DAPI (5mg/ mL in PBS) and slides were mounted using SlowFade Gold Antifade Mountant (Sigma Aldrich, S36937). The following antibodies and dilutions were used: TPRX1 1:200 (Merck, HPA044922), SOX2 1:300 (R&D systems, AF2018), H3.X/Y 1:200 (Active Motif, 61161). Secondary antibodies were Alexa Fluor conjugated and diluted 1:1000 (Molecular Probes). Single optical sections were captured with a Nikon A1-R (20x objective, 60x oil-immersion objective) or Carl Zeiss LSM780 microscope (63x oil-immersion objective). For visualization the images were pseudo-coloured and corrected for brightness and contrast (within the recommendations for scientific data) using Fiji (ImageJ 2.1.0/1.53c). Fluorescence semi-quantification analysis was performed with Volocity 6.3 (Improvision) on mid optical sections with manual segmentation.

Thawing, immunohistochemistry staining, and imaging of human embryos

Cryopreserved 4-8 cell stage human embryos were thawed using EmbryoThaw (FertiPro) according to manufacturer's instructions. After recovery in Cleave culture medium for an hour, zonae pellucidae were removed by brief incubation in acid Tyrodes solution and the embryos immediately fixed for 15 minutes with 4% paraformaldehyde. Immunofluorescence staining was performed as described previously (Roode et al., 2012). In brief, after, embryos were incubated for 15 minutes in PBS containing 3 mg/mL polyvinylpyrrolidone (PBS/PVP, P0930, SigmaAldrich), transferred to PBS/PVP+ 0.25% Triton X-100 (23,472-9, SigmaAldrich) for permeabilization for 30 minutes. Blocking for at least 1 hour, and all subsequent procedures were performed using PBS containing 0.1% BSA, 0.01% Tween 20 (P1379, SigmaAldrich) and 2% donkey serum. Antibodies against TPRX1 1:200 (Merck, HPA044922) and H3.X/Y 1:200 (Active Motif, 61161) were diluted in blocking buffer and embryos incubated overnight at 4°C. They were then

rinsed 3x in blocking buffer for at least 15 minutes per rinse, then incubated in secondary antibodies (Alexa Fluor conjugated, Molecular Probes) diluted 1:500 in blocking buffer for 1-2 hours at room temperature, rinsed in blocking buffer as previously, including DAPI to mark nuclei. After progression through increasing concentrations of Vectashield (H-1200, Vector Labs) in blocking buffer, they were mounted on glass slides in small drops of concentrated Vectashield. Coverslips were sealed with nail varnish. Multiple single optical sections of embryos were captured with a Carl Zeiss LSM780 microscope (63x oil-immersion objective). Composite images of multiple channels (fluorescent and/ or brightfield) were obtained by merging the individual channels using Fiji. Z-stacks (maximum intensity projections) of individual optical sections were generated using Fiji.

Quantitative reverse transcription PCR (qRT-PCR)

RNA from cells was isolated using RNeasy Mini kit (Qiagen, 74104) and treated with DNase (TURBO™ DNase 2U/ μL, Thermo Fisher Scientific, AM2238) according to manufacturer's protocols. 1ug of DNAase-treated RNA was used for cDNA synthesis using the RevertAid First-Strand cDNA Synthesis Kit (Thermo Fisher Scientific, K1622). The cDNA was diluted (1:10-20) and used for qRT-PCR in technical triplicate using Brilliant III SYBR master mix (Agilent Technologies, 600882) and CFX384 Touch Real-Time PCR Detection Systems (BioRad). Relative levels of transcript expression were quantified by the comparative ΔΔCt method with normalisation to RPL19 levels. Primer sequences are available in Table S4.

10X Single-cell RNA-seq library preparation

For 10X single-cell RNA-seq, the cells were dissociated by incubating with 0.25% trypsin for 10min at 37°C, followed by trituration by pipetting with 200ul tip. The cells were resuspended in DMEM/F12 supplemented with 0.1% BSA, washed twice and then filtered through 30μm mesh. 16,000 cells were resuspended in 47μl DMEM/F12 supplemented with 0.04% BSA. Single-cell RNA-seq libraries were prepared in the Cancer Research UK Cambridge Institute Genomics Core Facility using the following: Chromium Single Cell 3′ Library & Gel Bead Kit v3 (10X Genomics, PN-1000075), Chromium Chip B Kit (10X Genomics, PN-1000073) and Chromium Single Cell 3' Reagent Kits v3 User Guide (Manual Part CG000183 Rev C, 10X Genomics). Cell suspensions were loaded on the Chromium instrument with the expectation of collecting gel-beads emulsions containing single cells. RNA from the barcoded cells for each sample was subsequently reverse-transcribed in a C1000 Touch Thermal cycler (Bio-Rad) and all subsequent steps to generate single-cell libraries were performed according to the manufacturer's protocol with no modifications. cDNA quality and quantity were measured with Agilent TapeStation 4200 (High Sensitivity 5000 ScreenTape) after which 25% of material was used for gene expression library preparation. Library quality was confirmed with Agilent TapeStation 4200 (High Sensitivity D1000 ScreenTape to evaluate library sizes) and Qubit 4.0 Fluorometer (ThermoFisher Qubit™ dsDNA HS Assay Kit to evaluate dsDNA quantity). Each sample was normalized and pooled in equal molar concentration. To confirm concentration, pool was qPCRed using KAPA Library Quantification Kit on QuantStudio 6 Flex before sequencing. Pool was sequenced on S2 flowcell on Illumina NovaSeq6000 sequencer with following parameters: 28 bp, read 1; 8 bp, i7 index; and 91 bp, read 2.

10X Single-cell Multiome library preparation

For 10X single-cell Multiome sequencing, human naïve hESCs were dissociated by incubation with TrypLE for 10min at 37°C and flow sorted to remove dead cells and mouse feeder cells. Cells were lysed and nuclei were isolated according to the manufacturers' instructions: Nuclei Isolation for Single Cell Multiome ATAC + Gene Expression Sequencing protocol (CG000365_Rev A), and genomic DNA and RNA were processed with a Chromium Single Cell Multiome ATAC + Gene Expression kit. Single-cell RNA-seq and ATAC-seq libraries were prepared in the Babraham Institute Sequencing Facility using the following reagents and protocols: Chromium Next GEM Single Cell Multiome ATAC + Gene Expression Reagent bundle (PN-1000283), Chromium Next GEM Chip J Single Cell Kit (PN-1000234) and Chromium Next GEM Single Cell Multiome ATAC + Gene Expression User Guide (document code CG000338 Rev D). Nuclei were transposed in bulk solution in a Veriti 96-Well Thermal Cycler. The transposed nuclei suspensions were then loaded into a microfluidic chip and run in the Chromium Controller to generate Gel Beads-in-emulsion (GEMs) containing single nuclei. Incubation of the GEMs produced 10X barcoded DNA from transposed DNA fragments and 10X barcoded, full-length cDNA from RNA. All steps to produce single cell ATAC and gene expression libraries were performed according to the manufacturer's instructions. cDNA, ATAC library and gene expression library quantity and quality were assessed using the Agilent 2100 Bioanalyzer (High Sensitivity DNA chip). 10X Multiome ATAC-seq as well as RNA-seq samples were pooled (wildtype and *DUX4* overexpression each) and sequenced on an S1 flowcell on Illumina NovaSeq6000 at the CRUK-CI sequencing core facility (10X Multiome ATAC-seq: 50bp read length, index length 8bp + 24bp; 10X Multiome RNA-seq: 28bp read length, index length 10bp + 10bp).

Single-cell RNA-seq data analysis

Single-cell 10X RNA-seq samples were processed using the Cellranger count pipeline (v3.1.0) as Single Cell 3' (v3) data using default parameters and raw sequencing reads were aligned to the GRCh38 human genome. The resulting data were filtered based on the distribution of the counts of RNA features, expression of mitochondrial genes, and percent largest genes. In our dataset, only cells with more than 2.500 and less than 10.500 genes, as well as less than 10% mitochondrial reads, and less than 10% largest gene percentage were kept. The data were normalized, scaled, and variable features were identified using FindVariableFeatures function in Seurat (v4). PCA was performed based on variable features, UMAP was performed using the first 30 principal components and cells were clustered using Louvain at resolution 0.5. Differentially expressed genes between clusters were identified using the FindMarkers function (test.use="roc", only.pos = TRUE, logfc.threshold = 0.25). Plots were generated using DimPlot, DotPlot,

VlnPlot, FeaturePlot, FeatureScatter, DoHeatmap and DimHeatmap functions. Cell cycle analysis was performed using the CellCycleScoring function with default parameters. The naïve hESCs dataset was integrated with human embryo data (E3 – E7, E-MTAB-3929) using the functions FindIntegrationAnchors and IntegrateData function. Merged data were normalized, scaled, and clustered.

Transposable element analysis

Repeat family or subfamily 'repeatomes' were constructed using genome-wide annotation files of repeats generated by RepeatMasker (downloaded for the GRCh37 genome from the UCSC table browser). Individual instances of repeats were extracted from the genome sequence and concatenated together, whereby individual sequences were padded by NNNNN. To obtain FastQ files for single cells belonging to various clusters of interest, we used the cell level barcode files produced by Seurat (v4) as annotation files for subset10xbam (https://github.com/s-andrews/subset10xbam). This process uses the possorted BAM file outputted by CellRanger as well as the cell barcode annotations as input, and produces a new BAM file with entries only belonging to cells given in the annotation file as new output; during this process, the cell barcodes were added to the readID (option –add_barcode). These files were then converted to FastQ format (using samtools fastq, version 1.11), and split into individual single-cell FastQ files using a custom script (https://github.com/FelixKrueger/scRepeats). These single-cell FastQ files were then aligned to various repeat genome sequences using Bowtie2 (default parameters), whereby any alignment to a repeat family was scored. The results were then converted to percentage of total reads that aligned to a given repeat class/family.

Motif analysis

TF binding motifs overrepresented in our gene set were identified using RcisTarget with default parameters based on the hg19 database (version 1.10.0) (Aibar et al., 2017). Regions of 10kb centred around TSS of 8CLCs genes [top 200] were analysed and enriched motifs retrieved.

RNA velocity analysis

RNA velocity analysis was based on initial processing of the 10X RNA sequencing data using velocyto (v0.17) (La Manno et al., 2018) and further analysis using scVelo (v0.2.4) (Bergen et al., 2020). We used velocyto to generate a loom file from 10X cellranger output data ('velocyto run10x', see also https://velocyto.org/velocyto.py/tutorial/cli.html) that differentiates between spliced, unspliced, and ambiguous gene counts. This loom file was used for pre-processing and clustering via Seurat, and was then analyzed using scVelo (via an h5ad output file, see also https://scvelo.readthedocs.io/). Scvelo (mode='stochastic') was used to estimate trajectories based on spliced vs unspliced RNA for each cell and gene.

scATAC-seq data analysis

10X Multiome sequencing derived scATAC-seq data were analysed using ArchR (v1.0.1) (Granja et al., 2021). Fragment files were loaded to generate arrow files, filtered (min TSS enrichment = 8, min fragments = 3000, max fragments = 1e7), integrated with cell identities from scRNA-seq and bigwig files from pseudobulks (getGroupBW) were exported for visualization using IGV (see also https://github.com/rargelaguet/DUX4_8CLC_hESCs).

QUANTIFICATION AND STATISTICAL ANALYSIS

Statistics and reproducibility

Statistical tests, sample sizes and definitions of error bars of each experiment are indicated in the figure legends and were calculated using Graphpad Prism (version 9.2.0). For all tests, p values were presented as *$p<0.05$, **$p<0.01$, and ***$p<0.001$.